CHAPTER 9

Temperatures in Ice Masses

> "The action of heat is always present, it penetrates all bodies and spaces, it influences the processes of the arts, and occurs in all the phenomena of the universe."
>
> ***The Analytical Theory of Heat*, Joseph Fourier (1822)**[1]

9.1 Introduction

The temperature distribution in glaciers and ice sheets deserves attention both for its intrinsic interest and its relation to other processes. The present variation of temperature with depth provides information about past variations of surface temperature. The deformation rate of ice depends sensitively on temperature; cooling from $-10\,^{\circ}\mathrm{C}$ to $-25\,^{\circ}\mathrm{C}$ increases the viscosity by a factor of five. A glacier, previously frozen to its bed, starts to slip when its base warms to the melting point; the terminus then advances, perhaps unstably. The interaction between heat flow and ice flow adds considerable complexity to glacier dynamics and evolution. Properties such as the velocity of seismic waves and the absorption of radio waves, on which depend methods of measuring ice thickness, also vary with temperature. In particular, by scattering radio waves, water in the ice makes radar sounding difficult.

What controls the temperature distribution? Through the energy balance, the climate determines the surface temperature, as described in Chapter 5. Geothermal heat and frictional heating from basal slip warm or melt the base. Ice deformation and refreezing of meltwater warm the interior. Heat is transferred within the glacier by conduction, ice movement (advection), and, in some cases, water flow.

Geothermal, frictional, and deformational heat sources typically concentrate at or near the base of a glacier. The glacier itself is an effective thermal insulator. Thus the ice near the bed of a glacier tends to be comparatively warm. But the different heat sources and processes of transfer vary in importance. Moreover, glaciers thrive in a diverse range of climatic conditions. Consequently, four main types of temperature distributions occur:

1. All the ice is below melting point.
2. Only the bed reaches melting point.

[1] Translation by A. Freeman (1878).

DOI: 10.1016/B978-0-12-369461-4.00009-0

3. A basal layer of finite thickness is at melting point.

4. All the ice is at melting point except for a surface layer, about 15 m thick, where temperatures fluctuate with the seasons.

Glaciers with the first two types of distributions are said to be *cold*, those of the third type are called *polythermal*, and the last category is *temperate*. Reality is more complicated than this terminology suggests, however, for different types of temperature distributions may be found in different parts of the same glacier.

In this chapter we discuss the general problem of heat transfer in glaciers. But we first discuss the thermal properties of snow and ice, the factors controlling temperatures near the surface, and the characteristics of temperate glaciers.

9.2 Thermal Parameters of Ice and Snow

For a geological material, glacier ice is unusually pure. Consequently its thermal properties at subfreezing temperatures are well known from measurements on pure ice. Table 9.1 gives values obtained from a comprehensive data review by Yen (1981).

The following empirical formulae – expressed in S.I. units – relate the specific heat capacity c and thermal conductivity k_{T}^{i} of pure ice to the temperature T in Kelvin:

$$c = 152.5 + 7.122T \tag{9.1}$$

$$k_{\mathrm{T}}^{i} = 9.828 \exp\left(-5.7 \times 10^{-3} T\right). \tag{9.2}$$

Thermal conductivity also depends on density but the data are widely scattered, especially for snow with densities less than $500\,\mathrm{kg\,m^{-3}}$ (Sturm et al. 1997). The scatter arises because conductivity depends on snow texture, which influences the area of contact between adjacent ice grains (Adams and Sato 1993). Textures range from small rounded grains to large faceted crystals. The following formulae can be used for thermal conductivity of dry snow, firn, and ice. The Van Dusen (1929) formula,

$$k_{\mathrm{T}} = 2.1 \times 10^{-2} + 4.2 \times 10^{-4}\rho + 2.2 \times 10^{-9}\rho^{3}, \tag{9.3}$$

Table 9.1: Values for thermal parameters of pure ice.

		Temperature	
		0 °C	−50 °C
Specific heat capacity	J $kg^{-1}K^{-1}$	2097	1741
Latent heat of fusion	kJ kg^{-1}	333.5	
Thermal conductivity	W $m^{-1}K^{-1}$	2.10	2.76
Thermal diffusivity	$10^{-6}m^{2}s^{-1}$	1.09	1.73

gives a lower limit in most cases. Low-density hoar layers, however, can be even less conductive (Sturm and Johnson 1992). The Schwerdtfeger (1963) formula,

$$k_{\mathrm{T}} = \frac{2k_{\mathrm{T}}^{i}\rho}{3\rho_i - \rho}, \tag{9.4}$$

gives an upper limit. The specific (per unit mass) heat capacity of dry snow and ice does not vary with density because the heat needed to warm the air and vapor between the grains is negligible. Thermal diffusivity, α_{T}, can be calculated for any density and temperature using $\alpha_{\mathrm{T}} = k_{\mathrm{T}}/\rho c$.

9.3 Temperature of Surface Layers

The penetration of seasonal and long-period changes in surface temperature can be analyzed by heat conduction theory. Fourier's law of heat conduction states that the heat flux q (the amount of heat energy flowing across unit area in unit time) at a point in a medium is proportional to the temperature gradient $\partial T/\partial z$, with z measured in the direction of the temperature variation. Thus

$$q = -k_{\mathrm{T}}\frac{\partial T}{\partial z}, \tag{9.5}$$

where k_{T} denotes the thermal conductivity. The minus sign indicates that heat flows in the direction of lower temperatures.

Consider an element of unit cross-section and thickness δz in a material at rest. Call the heat flowing in one side q; out of the other side flows $q + [\partial q/\partial z]\delta z$. If $\partial q/\partial z$ is positive, more heat flows out than in, so the element cools. By the definition of specific heat capacity c, the change in heat in unit time equals $-\rho c[\partial T/\partial t]\delta z$ where ρ is density and t the time. It follows that, for constant k_{T},

$$-\rho c\frac{\partial T}{\partial t} = \frac{\partial q}{\partial z} = -k_{\mathrm{T}}\frac{\partial^2 T}{\partial z^2}, \qquad \text{or}$$

$$\frac{\partial T}{\partial t} = \alpha_{\mathrm{T}}\frac{\partial^2 T}{\partial z^2}. \tag{9.6}$$

The proportionality $\alpha_{\mathrm{T}} = k_{\mathrm{T}}/\rho c$ defines the thermal diffusivity.

Consider a cyclic variation of temperature at the surface ($z = 0$), with fluctuations about the mean value following

$$T(0, t) = A_{\mathrm{T}}\sin(2\pi\omega t). \tag{9.7}$$

A_{T} denotes the amplitude and ω the frequency (cycles per time) of the variation. The solution of Eq. 9.6 gives the temperature variation in the subsurface at depth z as

$$T(z, t) = A_{\mathrm{T}}\exp\left(-z\sqrt{\pi\omega/\alpha_{\mathrm{T}}}\right)\sin\left(2\pi\omega t - z\sqrt{\pi\omega/\alpha_{\mathrm{T}}}\right). \tag{9.8}$$

This solution shows that:

1. The amplitude of the wave decreases as $\exp\left(-z\sqrt{\pi\omega/\alpha_T}\right)$. Thus, the higher the frequency, the more rapid the attenuation with depth. In reality, surface temperature variations are a complicated function of time. They can, however, be expressed as harmonic series. The higher harmonics attenuate most rapidly, and the temperature perturbation at depth approximates a wave of the fundamental frequency. For example, at one-meter depth in cold firn the temperature variations mostly reflect the seasonal cycle, even though large weekly temperature changes occur at the surface. This pattern is seen in field measurements (Figure 9.1).

2. Temperature maxima and minima propagate at a velocity $2\sqrt{\pi\omega\alpha_T}$.

Table 9.2 lists some numerical values. Figure 9.2 shows the seasonal variations in near-surface temperatures. Field observations confirm that seasonal variations are undetectable below a depth of about 20 m. In contrast, Table 9.2 suggests that the 100 kyr ice-age temperature cycle penetrates to the base of an ice sheet, a process we discuss later.

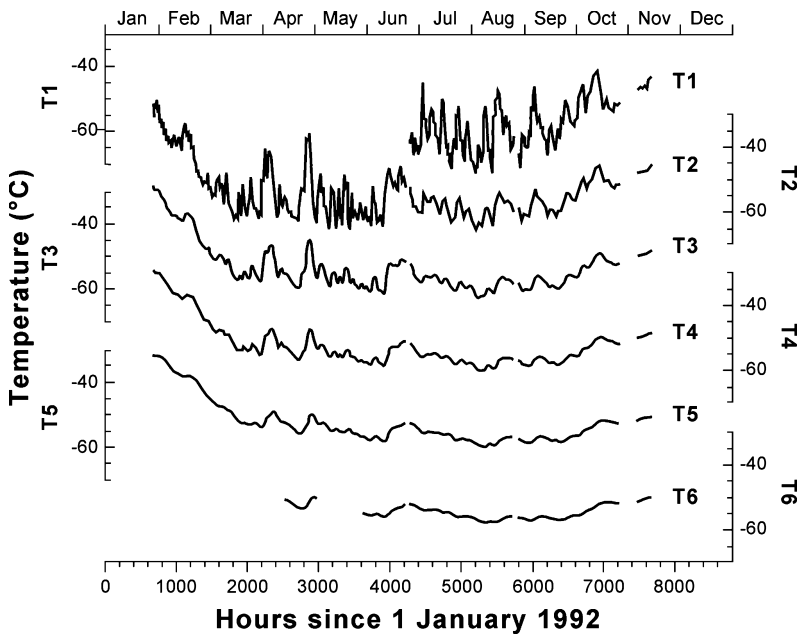

Figure 9.1: Variation of temperature over 10 months at South Pole, at six depths in the near-surface firn. At the end of the experiment, the depths of the six thermistors (called T1 through T6) were about 0.2, 0.4, 0.6, 0.8, 1.0, and 1.2 meters. Due to snowfall, the depths increased by about 0.4 m over the year, beginning around hour 3500. Temperature variability decreases with depth. Adapted from Brandt and Warren (1997).

Table 9.2: Propagation by conduction of a cyclical variation in surface temperature.

P_ω(yr)	z_5(m)	v(m yr^{-1})	Δt(yr)
1	10.2	21.3	0.48
2500	509	0.427	1192
10^5	3220	0.067	4.8×10^4

P_ω = period = ω^{-1}.
z_5 = depth at which amplitude is 5% of surface value.
v = velocity of propagation of maxima and minima.
Δt = time lag = z_5/v.

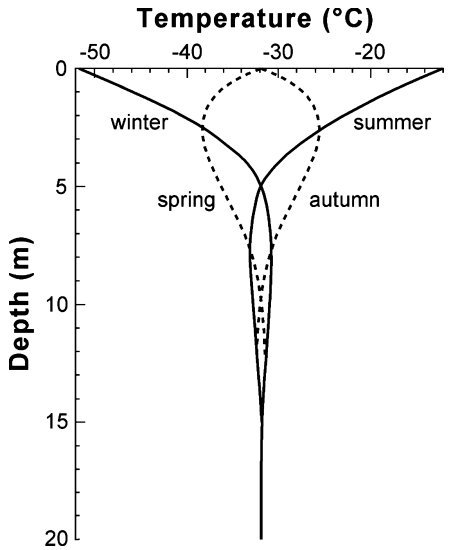

Figure 9.2: Theoretical seasonal cycle of firn temperatures in central Greenland.

In summer, in most places, heat conduction plays only a minor part in heat transfer through the surface layers. Except in the interiors of Greenland and Antarctica or on very high mountains the surface melts in summer and might receive rain. Surface water percolates into the snow and refreezes when it reaches a depth where the temperature remains below melting point. Refreezing of 1 g of water produces enough heat to raise the temperature of 160 g of snow or firn by 1 °C. (the ratio of the latent heat to the specific heat capacity is 160). This process significantly warms the layers near the surface. Figure 9.3 illustrates changes in temperature of the firn at a location on the Greenland Ice Sheet, at about 1600 m elevation on the EGIG survey line (data of N. Humphrey). The firn at 3 to 4 m below the surface warms rapidly, by 8 °C in just 6 days, because meltwater percolates down and refreezes. This process eliminates the winter's "cold wave" much more quickly than would have been possible by heat conduction alone. Cai et al. (1986) and Pfeffer and Humphrey (1996) have made mathematical analyses of this process. The latter study

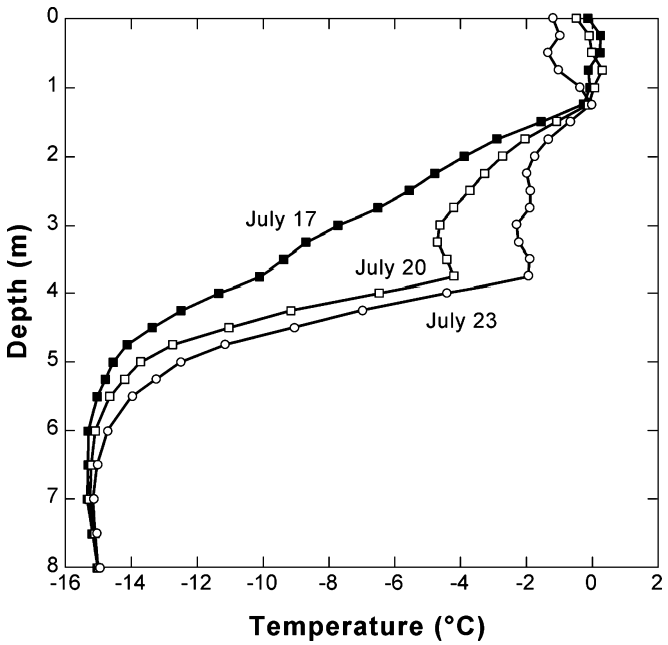

Figure 9.3: Warming of firn by latent heat of refreezing meltwater, at 1600 m elevation on the Greenland Ice Sheet. Data courtesy of N. Humphrey and T. Pfeffer.

also compared measured temperatures to strata in the firn and showed that warming initially concentrates in layers with growing ice lenses.

It is often stated that the temperature measured at a depth of 10 or 15 m in a glacier, beneath the zone of seasonal variation, equals the mean annual air temperature. Though not true in general, this is a good approximation at many cold, dry sites where the maximum air temperature never rises to 0 °C. A comparison of air and 10 m firn temperatures at polar dry-snow locations indicates that, at most sites, the two differ by less than 2 °C (Table 9.3). Firn temperatures are colder on average by only 0.7 °C.

In other cases, the air and firn temperatures differ substantially. Refreezing of surface water warms the firn and raises its temperature above the mean annual value for the air. Measurements at two glaciers in the Alps, for example, found a 0 °C temperature at 30 m depth, even though the mean annual air temperature at both sites was −7 to −8 °C (Hughes and Seligman 1939; Lliboutry 1963). Such warming is not effective in the ablation zone, where most surface water escapes from the glacier. This explains why, in polar glaciers, near-surface temperatures can be lower in ablation zones than accumulation zones, despite their lower altitude (Table 9.4).

On the other hand, warming of the firn in areas of melt is restricted because the glacier surface temperature cannot rise above 0 °C, even if the air temperature does. In contrast, winter snow acts as a blanket that reduces heat loss. Winter snow thus warms the ice, especially in the ablation area; in the accumulation area the net warming is weaker because some of the snow

Table 9.3: Mean annual air temperature and temperature at 10 m depth in dry-snow areas.

Location	Latitude	Longitude	Temperature (°C)	
			Air	Firn
Camp Century	77.2°N	61.1°W	−23.5	−24.5
Site 2	77.1°N	56.1°W	−24.1	−24.1
Station Centrale	70.9°N	40.6°W	−28.3	−27.6
Northice	78.1°N	38.5°W	−30.0	−28.0
Byrd	80.0°S	120.0°W	−28.2	−28.3
Pionerskaya	69.7°S	95.5°E	−38.0	−39.4
South Pole	90.0°S		−49.3	−50.8
Vostok	78.5°S	106.8°E	−56.0	−57.3
Plateau	79.3°S	40.5°E	−56.6	−60.2

Table 9.4: Temperatures at different points in same glacier.

Glacier	Zone	T (°C)	Depth (m)
Jackson Ice Cap[‡]	firn accumulation ice accumulation ablation	−3 −9 −8 to −10.5[†]	20 20 20
Vestfonna Ice Cap[‡]	accumulation ablation	−3 −7 to −10[†]	14 10

[†] Measured at various elevations.
[‡] Franz Josef Land.
[‡] Spitsbergen.
Data from Krenke (1963) and Schytt (1964).

becomes part of the glacier. Other features that produce local temperature variations include water channels within the ice and crevasses. The latter collect water in summer and cold air in winter. In the heavily crevassed shear margin of Whillans Ice Stream, West Antarctica, the ponding of cold winter air depresses mean annual temperatures by about 12 °C at a depth of 30 m (Harrison et al. 1998).

9.4 Temperate Glaciers

9.4.1 Ice Temperature

The definition of a temperate glacier in the introduction is not precise and the often-used term *pressure melting point* misleads; because the ice contains impurities it does not have a distinct melting point, determined solely by pressure. Temperate ice is a complex material consisting of ice, water, air, salts, and carbon dioxide. The water content usually ranges between 0.1% and 2% (Lliboutry 1976). Most of the water occupies the intersections of three or four grains, but it

also occurs in lenses on grain boundaries, around air bubbles, and at salt inclusions. Air bubbles typically comprise a few percent of the ice volume. The impurities are distributed between the liquid in the veins along three-grain intersections, the grain-boundary area excluding the veins, and the bulk of the ice (Harrison and Raymond 1976). Although the bulk impurity content is only of the order 10^{-7} by weight, the impurities concentrate enough in the liquid in the veins to affect the equilibrium temperature.

If temperate ice were a mixture of pure ice and pure water, its temperature T at absolute pressure P would be

$$T = T_o - \mathcal{B}P, \tag{9.9}$$

where $\mathcal{B} = 7.42 \times 10^{-8}\text{K Pa}^{-1}$ specifies the rate of change of melting point with pressure, and $T_o = 273.16\text{ K} = 0.01\,^{\circ}\text{C}$ denotes the triple-point temperature of water. Strictly speaking, P should be measured relative to its value at the triple point, but this pressure is small enough (600 Pa) to be neglected. Because glacier ice contains air bubbles, the water in it should probably be regarded as air-saturated rather than pure. Dissolved air at atmospheric pressure lowers the equilibrium temperature by $2.4 \times 10^{-3}\,^{\circ}\text{C}$. Moreover, solubility increases in proportion to pressure. Equation (9.9) should therefore be replaced by

$$T = T_o - \mathcal{B}'P, \tag{9.10}$$

where $\mathcal{B}' = 9.8 \times 10^{-8}\text{K Pa}^{-1}$ or $8.7 \times 10^{-4}\text{K m}^{-1}$ of ice. Stress in a glacier deviates from hydrostatic and this introduces a further complication; P is not necessarily the hydrostatic pressure but rather the stress normal to the liquid-solid interface (LaChapelle 1968; Kamb 1961).

Impurities depress the melting point in proportion to the solute concentration in the liquid inclusions. For small concentrations, this shifts the temperature by $-\mathcal{B}_s C_s / W$, for a fractional water content W by weight, and salt concentration C_s in mol kg^{-1}, and $\mathcal{B}_s = 1.86\text{ K kg mol}^{-1}$ (Lliboutry 1976). Thus the equilibrium temperature of the ice is

$$T = T_o - \mathcal{B}'P - \frac{\mathcal{B}_s C_s}{W}. \tag{9.11}$$

Curvature of the ice-water interface also influences equilibrium temperature but by a small amount compared to impurities (Lliboutry 1976).

Impurities greatly increase the effective specific heat capacity of ice near the melting point (Harrison 1972). The concentration of salt solution in equilibrium with ice depends on the temperature. Only part of the heat added to the ice raises the temperature – some of it must melt ice to dilute the liquid. The effective specific heat capacity c' thus exceeds the value for pure ice, c:

$$c' = c + L\frac{dW}{dT}, \tag{9.12}$$

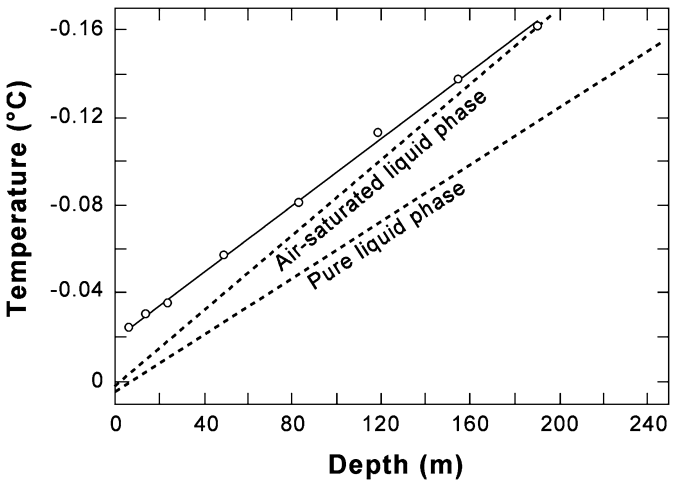

Figure 9.4: Variation of temperature with depth in the temperate Blue Glacier (solid line) and variation expected for pure ice in equilibrium with (a) pure water and (b) air-saturated water. Impurities depress the melting point in the glacier. Redrawn from Harrison (1975).

where L denotes the specific latent heat of fusion, and W is related to T by Eq. 9.11. For typical salt concentrations and $T = -0.01\,^{\circ}\mathrm{C}$, c' can be about one hundred times c. Air bubbles have the same effect as salts (Raymond 1976).

Harrison (1972) proposed a precise definition of temperate ice, based on the concept of effective specific heat capacity: "Temperate ice is ice whose effective bulk heat capacity is significantly greater than that of a pure ice monocrystal." A single crystal is specified to eliminate grain-boundary effects.

Figure 9.4 shows temperatures measured in two boreholes in Blue Glacier, Washington. The glacier is colder than predicted by Eqs. 9.9 and 9.10, due to effects of impurities and air bubbles. In a temperate glacier borehole, the temperature of the water obeys Eq. 9.10, since the solute bulk concentration is negligible; in contrast, the surrounding ice has the colder values given by Eq. 9.11. Thus a water-filled borehole in temperate ice loses heat to the glacier and will refreeze at all depths. This has been observed.

9.4.2 Origin and Effect of Water

For a glacier to be temperate, it must contain heat sources and sinks. These are provided by the freezing of small quantities of water and the melting of small quantities of ice. In the accumulation zone, for example, a parcel of ice experiences an ever-increasing pressure as subsequent snowfalls bury it; its melting temperature therefore decreases and it must cool by giving up heat, which melts a small amount of ice. As ice flows toward the surface in the ablation zone, in contrast, the pressure on a given parcel decreases and so its melting temperature increases. If the ice is to remain temperate, it must be heated.

In a temperate glacier, conduction downward from the surface carries an insignificant amount of heat because the vertical temperature gradient is so small. The direction of this temperature gradient prevents heat conduction from the bed; all the basal heat melts ice there (typically about $1\,\mathrm{cm\,yr^{-1}}$). Deformation produces some heat within the glacier but only in about the lower half of the ice thickness is it sufficient to maintain the ice at melting point (Paterson 1971). The necessary heat must therefore be supplied by the freezing of the small quantities of water in the ice.

The water dispersed throughout a temperate glacier, which typically comprises about 1% of the volume, has various sources: percolation and conduit flow from the surface, ice melted by deformational heating, melting induced by pressure changes, and pockets of water trapped when the ice formed. What is their relative importance? Near the base of temperate glaciers, where the shear stress is about 100 kPa and the shear strain rate may be about $0.2\,\mathrm{yr^{-1}}$, the heat of deformation could melt about 1% of the ice in 100 yr. This mechanism cannot, however, produce this amount of water throughout the bulk of the ice. Paterson (1971) estimated the amounts of water produced by the other sources in Athabasca Glacier and concluded that most of the water was trapped when firn became ice. It does not drain away because the intergranular permeability of temperate ice is extremely low (Chapter 6). Temperature measurements such as those in Figure 9.4 confirm that permeabilities are low; they demonstrate that impurities are not flushed out of the ice. Large quantities of water move through temperate glaciers in fractures, tubes, and other large passageways (Chapter 6). This water carries some heat into the glacier, and a portion of it might freeze. Because such passageways occupy only a small volume of the glacier, their effect on temperatures is often assumed to be negligible, but this topic needs more investigation.

9.4.3 Distribution of Temperate Glaciers

Temperate glaciers are widespread in the literature; how widespread they are in reality is uncertain. It is often assumed that all glaciers in temperate regions are temperate. This is certainly untrue.

For a glacier to be temperate, the previous winter's cold wave must be eliminated by the end of summer. Refreezing of percolating meltwater can accomplish this rapidly in the accumulation zone (Figure 9.3). In the ablation zone, however, the ice is almost impermeable to water. Paterson (1972b) discussed other processes. Heat conduction is slow and the amount of heat is limited because the surface temperature cannot rise above 0 °C. Solar radiation does not penetrate deeply enough. Most of the heat at the surface warms the surface ice to 0 °C and then melts it. Whether all the ice attains 0 °C by the end of the summer therefore depends largely on the amount of ablation relative to the depth of penetration of the cold wave, a function of winter temperatures and snowfall. In many glaciers the ice likely remains below melting point in the region of slow ablation immediately below the equilibrium line.

Haeberli (1976) reviewed temperature data from glaciers in the Alps, where accumulation zones at high elevations are not temperate. On Mont Blanc, for example, 15 m temperatures are about −17 °C at 4785 m elevation and about −7 °C at 3960 m. Rapid transport of such cold ice may bring it into ablation zones while still subfreezing. Nonetheless, the ice is probably temperate in the lower parts of major glaciers with high ablation rates.

The most likely place to find temperate glaciers is a region with a maritime-temperate climate where intense summer melting follows heavy winter snowfalls. This describes the setting of Blue Glacier, located 75 km from the Pacific Ocean at latitude 48°N in Washington. Here, LaChapelle (1961) found that subfreezing temperatures never penetrated below 4 m in the accumulation zone in winter, and the firn temperature never fell below −2 °C. Summer melt and rain soon remove this small cold wave. Measurements just below the equilibrium line revealed temperate ice there too (Harrison 1975). On the other hand, Mathews (1964) measured temperatures of about −2 °C in a tunnel under South Leduc Glacier, in western Canada, located 100 km from the coast at latitude 56°N.

In polar regions, some glaciers may have temperate accumulation zones as a result of percolating meltwater, while the ablation zones are cold. Schytt (1969) described this situation in Svalbard: "In many glaciers, previously considered as temperate . . . the cooling starts just above the equilibrium line and the ice temperature in the upper several tens of metres stays below 0 °C all the way to the ice edge."

9.5 Steady-state Temperature Distributions

The temperature distribution in a glacier is never in a steady state, but heat flow rapidly reduces large deviations from a steady pattern. A large part of measured temperature profiles can therefore be understood by examining steady-state distributions.

9.5.1 Steady-state Vertical Temperature Profile

Within a glacier, conduction transfers heat both vertically and horizontally, but small temperature gradients usually make the latter negligible. Heat transfer by ice flow, however – the "advection" – is important both horizontally and vertically. Ice moving vertically (z-direction) with velocity w carries a heat flux $\rho c w T$ across a plane of unit area, oriented perpendicular to z. This term must be added to q in Eq. 9.6. A similar term must be included for advection due to ice flow at rate u in the horizontal direction x (choosing x to follow a flow line). Equation 9.6 thus becomes

$$\frac{\partial T}{\partial t} = \alpha_{\mathrm{T}} \frac{\partial^2 T}{\partial z^2} - w \frac{\partial T}{\partial z} - u \frac{\partial T}{\partial x}. \tag{9.13}$$

In thermal steady state, $\partial T/\partial t = 0$. Because the temperature would not remain constant if the ice thickness or velocity changed, the ice sheet is also implicitly assumed to be in a steady state of flow and geometry. In steady state, the temperature profile along a given vertical line, fixed in space, remains unchanged as the ice flows by.

9.5.1.1 Steady State with No Horizontal Advection

We first consider a case with negligible horizontal advection, with parameters appropriate for an ice sheet. Robin (1955) obtained the steady-state solution as follows. Position the origin at the base of the ice, assumed flat, and point the x-axis horizontally in the direction of flow. The z-axis is vertical and positive upward. This coordinate system is fixed in space. No ice or heat flows in the transverse direction. The following simplifying assumptions are made:

1. Horizontal conduction can be neglected because the horizontal temperature gradient is small compared with the vertical one. The term $u\partial T/\partial x$ cannot be neglected, in general, because, although $\partial T/\partial x$ is small compared with $\partial T/\partial z$, u is normally much greater than w. In Robin's analysis it is neglected, however; the solution should therefore apply near an ice sheet divide, where u is small.
2. The firn layer is replaced by an equivalent thickness of ice.
3. The heat generated by ice deformation is treated as a flux, additional to the geothermal flux, at the base of the ice. This is a reasonable approximation because, in the slow-flowing parts of ice sheets, most of the shearing occurs near the base.
4. The base is colder than melting point.

The assumptions reduce the steady-state heat-transfer equation to

$$\alpha_{\mathrm{T}}\frac{d^2T}{dz^2} - w\frac{dT}{dz} = 0. \tag{9.14}$$

Let H signify the ice thickness. The boundary conditions are, at $z = H$, $T = T_s$, a constant; at $z = 0$, heat flux $= -k_{\mathrm{T}}[dT/dz]_B =$ constant. One integration gives

$$\frac{dT}{dz} = \left[\frac{dT}{dz}\right]_B \exp\left(\frac{1}{\alpha_{\mathrm{T}}}\int_0^z w\,dz\right). \tag{9.15}$$

To proceed further, w needs to be expressed as a function of z. At the surface w must balance the accumulation (or ablation) to keep the ice sheet in a steady state. At the base w must be zero in the absence of melting. So we take $w = -\dot{b}_i z/H$, with the surface specific mass balance rate $\dot{b}_i$ expressed as thickness of ice per unit time. Integration of Eq. 9.15 using this relation for w gives

$$T - T_B = \left[\frac{dT}{dz}\right]_B \int_0^z \exp\left(-z^2/z_*^2\right) dz, \tag{9.16}$$

with $z_*^2 = 2\alpha_T H/\dot{b}_i$. When $\dot{b}_i > 0$, this can also be written

$$T - T_s = z_* \frac{\sqrt{\pi}}{2} \left[\frac{dT}{dz}\right]_B [\mathrm{erf}\,(z/z_*) - \mathrm{erf}\,(H/z_*)], \tag{9.17}$$

in which erf stands for the error function,

$$\mathrm{erf}(z) = \frac{2}{\sqrt{\pi}} \int_0^z \exp\left(-y^2\right) dy. \tag{9.18}$$

Figure 9.5 illustrates such temperature distributions in terms of the dimensionless variables:

Distance above the bed:

$$\xi = \frac{z}{H} \tag{9.19}$$

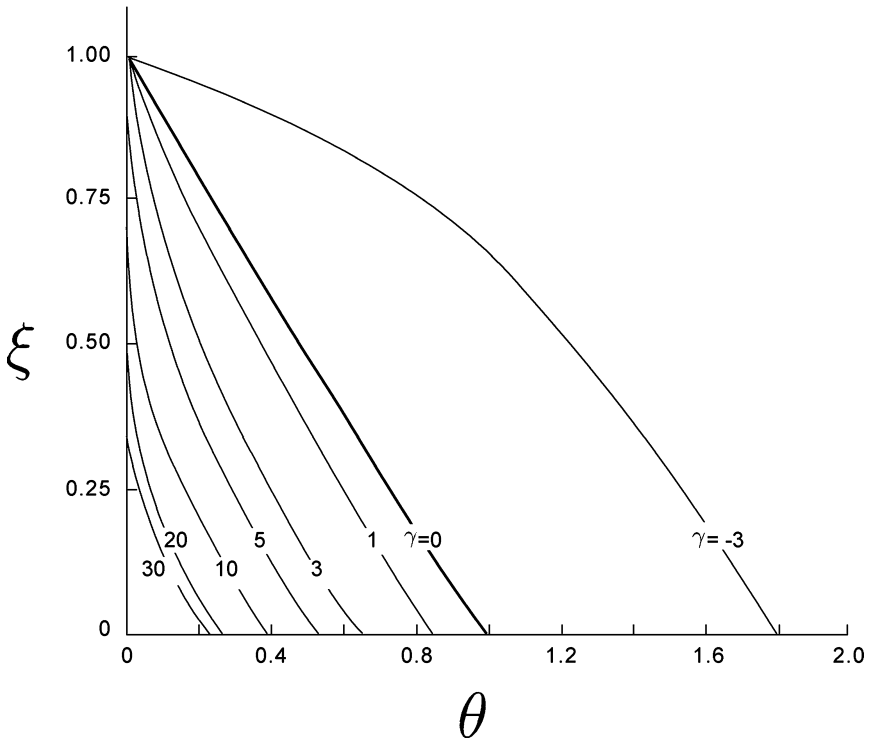

Figure 9.5: Dimensionless steady temperature profiles for various values of the advection parameter (γ). Negative value for γ indicates upward velocity; positive values indicate downward velocity. Equations 9.19–9.21 define the variables; θ refers to scaled temperature and ξ to scaled height above the bed. Adapted from Clarke et al. (1977) and used with permission of the American Geophysical Union, *Reviews of Geophysics and Space Physics*.

Temperature:

$$\theta = \frac{k_{\mathrm{T}}\,[T - T_s]}{GH} \tag{9.20}$$

Advection parameter:

$$\gamma = \frac{\dot{b}_i H}{\alpha_{\mathrm{T}}} \tag{9.21}$$

The advection parameter γ is, apart from a minus sign in cases of ablation, the same as the *Péclet Number*, a general indicator of the relative importance of advection and conduction. The dimensionless temperature depends on the geothermal flux G, a positive number. In a region of accumulation $\dot{b}_i > 0$. The temperature difference between surface and bed is given by the value of θ at the bed:

$$\theta_B = \left[\frac{\pi}{2\gamma}\right]^{1/2} \mathrm{erf}\,(\gamma/2)^{1/2}. \tag{9.22}$$

For $\gamma > 6.5$, corresponding to $\theta_B < 0.49$, $\mathrm{erf}\,(\gamma/2)^{1/2} \approx 1$, so that $\theta_B = (\pi/2\gamma)^{1/2}$, Figure 9.5 demonstrates that the vertical flow of ice profoundly affects the temperature distribution. In the absence of accumulation or ablation, the temperature-depth profile follows a straight line with slope equal to the geothermal gradient. Downward ice flow, corresponding to accumulation, carries cold ice from the surface and thus decreases the temperature. Ablation carries warm ice upward and increases the temperature. Note that, by Eq. 9.15, the maximum temperature gradient occurs at the bed in the accumulation zone but at the surface in the ablation zone. For $\dot{b}_i = 0.025\,\mathrm{m\,yr^{-1}}$ and $H = 3.5\,\mathrm{km}$, typical values for central East Antarctica, $\gamma = 2.5$ and $\theta_B = 0.7$. For an average geothermal heat flux ($50\,\mathrm{mW\,m^{-2}}$) the temperature difference between surface and bed is 59 °C. For central Greenland, $\dot{b}_i = 0.25\,\mathrm{m\,yr^{-1}}$, $H = 3\,\mathrm{km}$, $\gamma = 21$, $\theta_B = 0.27$, and the temperature difference drops to 20 °C. In Greenland, geothermal heat only affects the lower half of the ice sheet; the upper half is isothermal, as depicted in Figure 9.5. Now consider an ablation zone example: for $\dot{b}_i = -0.5\,\mathrm{m\,yr^{-1}}$, $H = 400\,\mathrm{m}$, and $\gamma = -5.5$, then $T_B - T_s = 36\,^{\circ}\mathrm{C}$. Because few, if any, glaciers have surface temperatures as low as $-36\,^{\circ}\mathrm{C}$ in the ablation zone, this calculation suggests that most glaciers, even in the Arctic, tend to reach melting point at their bases in the ablation zone. Whether they do or not depends also on the horizontal advection, not considered in this analysis.

In ice shelves and glaciers that slide rapidly, basal melting cannot be neglected. If $\dot{b}_b$ denotes the ice thickness removed in unit time at the bed (not the mass as in Chapter 4), the temperature distribution is obtained by integrating Eq. 9.15 using

$$w = -\dot{b}_b - \left[\dot{b}_i - \dot{b}_b\right] \frac{z}{H}. \tag{9.23}$$

At an ice divide, the downward flow of ice is slower, for the same depth, than at locations away from the divide (Raymond 1983; see Chapter 8). This reduces the cooling influence of

vertical advection and increases the basal temperature; a "warm spot" should be found under the divide. Using the relation for w for an ice divide suggested by Raymond, $w = -\dot{b}_i z^2/H^2$, rather than the linear one, gives a modified form of Eq. 9.16:

$$T - T_B = \left[\frac{dT}{dz}\right]_B \int_0^z \exp\left(-z^3/\zeta^3\right) dz, \tag{9.24}$$

with $\zeta^3 = 3\alpha_T H^2/\dot{b}_i$. For $\dot{b}_i = 0.25\,\mathrm{m\,yr^{-1}}$, $H = 3\,\mathrm{km}$, and $G = 50\,\mathrm{mW\,m^{-2}}$, $T_B - T_s = 27\,^\circ\mathrm{C}$, compared with 20°C derived from Eq. 9.16. This reveals a sensitivity of the temperature distribution to the form of $w(z)$, an important point because very few measurements have been obtained of vertical velocity profiles in ice sheets.

9.5.1.2 Effect of Horizontal Advection

Except near an ice divide, horizontal advection usually exerts a strong influence on temperature profiles; the term $-u\partial T/\partial x$ in Eq. 9.13 needs to be included. Temperatures tend to increase in the direction of glacier flow, because the surface elevation declines. Along the surface, temperature typically increases by 0.4 to 1 °C per 100 m drop in altitude. Glacier flow thus transports colder ice, originating at higher altitudes, into warmer regions – horizontal advection usually reduces temperatures. Figure 9.6 illustrates the effects of horizontal advection, using numerical solutions to Eq. 9.13.

Such cooling does not alter the surface temperature, which is fixed by climate, but depresses the temperature at depth. If sufficiently strong, horizontal advection causes the temperature to decrease with increasing depth, a situation usually referred to as a "negative temperature gradient." Yet geothermal and frictional heat sources still warm the bed, so the net imprint of horizontal advection is a cold spot in the central to upper part of the ice column (Figure 9.6). The "cold spot" is cold *relative* to the profile expected in the absence of horizontal advection (Figure 9.5); a negative temperature gradient does not necessarily develop.

Horizontal advective cooling is strongest where flow is fast and the glacier surface steep. But faster flow also usually increases heat sources from basal friction and ice deformation. Deep in the glacier, such increased heating counteracts the cooling effect of advection (Figure 9.6). The combination of heating near the bed and cooling in mid to upper layers increases the temperature gradient $\partial T/\partial z$ in the lower half of the ice thickness, sometimes by a large amount.

9.6 Measured Temperature Profiles

Figure 9.7 shows some measured temperature profiles in ice sheets and ice caps. Data sources are Vostok, Antarctica (Salamatin et al. 2008); Bindschadler Ice Stream, Antarctica (Engelhardt 2004b); Siple Dome, Antarctica (Engelhardt 2004a); Jakobshavn margin, west Greenland (Lüthi et al. 2002); GISP2, central Greenland (Cuffey et al. 1995); NGRIP, north-central Greenland (Dahl-Jensen et al. 2002); Byrd Station, Antarctica (Gow et al. 1968); Devon Island ice cap,

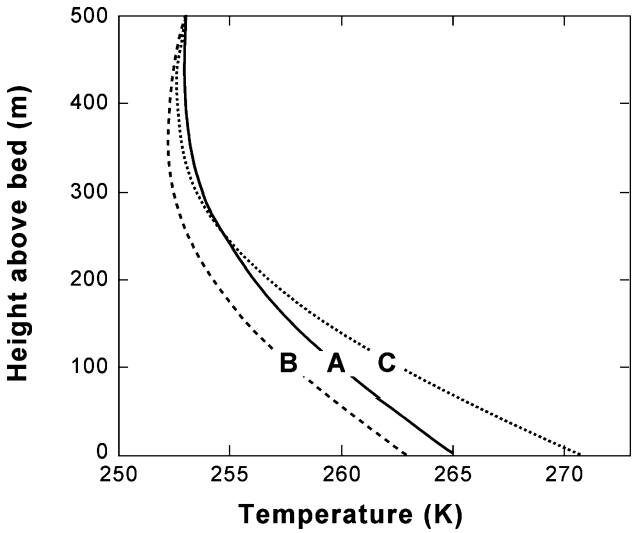

Figure 9.6: Theoretical influence of horizontal advection on the profile of temperature with depth. This example corresponds to the accumulation zone of a 500-m-thick glacier, with 0.4 m yr^{-1} of accumulation and surface velocity of 20 m yr^{-1}. (At depth, the velocity decreases according to the theoretical profile for flow by internal deformation.) Case A: Horizontal flow cools the ice because of an along-glacier temperature gradient of 0.12 °C km^{-1}, but also warms basal layers by frictional heating. Increasing the along-glacier temperature gradient to twice the value in A gives Case B. Temperatures are reduced at all depths, and a "negative temperature gradient" forms in the upper layers. Increasing the ice velocity to 40 m yr^{-1}, but leaving the temperature gradient as in A, gives Case C. Advective cooling and frictional heating both strengthen in this case; the basal zone warms, upper layers cool.

Arctic Canada (Paterson and Clarke 1978). The basal ice has reached melting point at Byrd Station, Bindschadler Ice Stream, Vostok, NGRIP, and Jakobshavn.

Profiles from sites with slow horizontal flow (Vostok, GISP2, NGRIP, Byrd, Siple Dome, and Devon) all show the features of the theoretical curves in Figure 9.5 for the appropriate value of the advection parameter. The Vostok and Siple Dome profiles are close to linear, as expected at dry locations with small vertical velocities. Vertical advection is much greater at the central Greenland sites (GISP2 and NGRIP) and Byrd station; both display nearly isothermal upper layers. Refreezing of percolating meltwater near the surface explains isothermal conditions in the top 80 m of the Devon Island profile.

The Bindschadler Ice Stream (formerly, Ice Stream D) and Siple Dome profiles belong to the same region in Antarctica. Yet they differ greatly because Bindschadler Ice Stream flows rapidly, about 350 m yr^{-1}. It shows the effects of horizontal advection, as expected from the theoretical curves in Figure 9.6: cooler ice at mid-depths and a steeper temperature gradient near the bed. Here, however, the steep basal gradient reflects not only increased heat generation at the

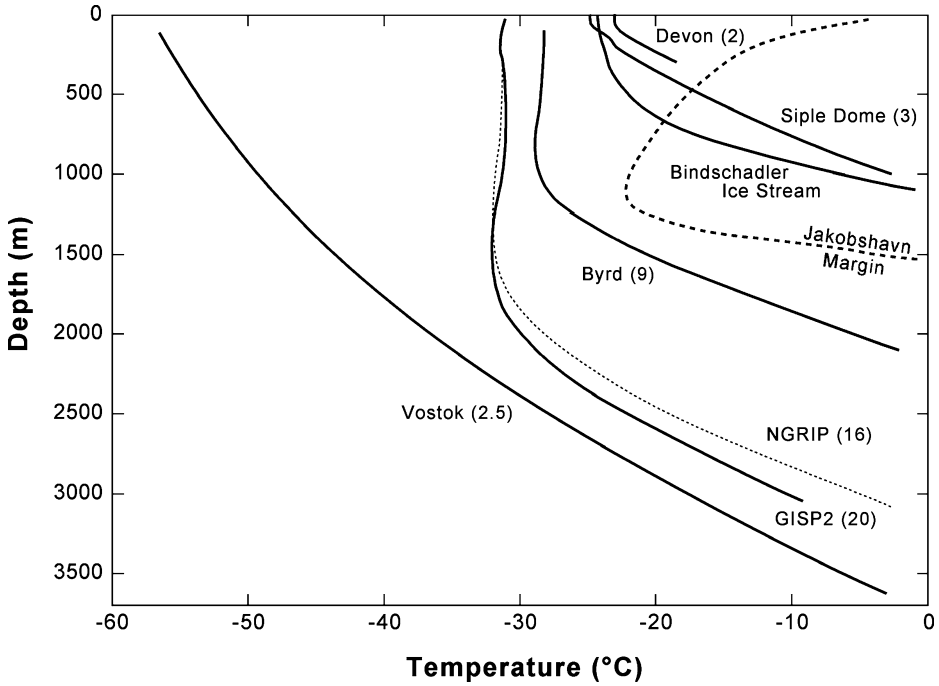

Figure 9.7: Measured temperature profiles in accumulation zones of polar ice sheets and ice caps. For sites with negligible horizontal advection, the number in parentheses gives the advection parameter defined by Eq. 9.21. Data sources are given in the text.

bed, but also vertical thinning of the ice as it passes from the central ice sheet to the thinner, faster-flowing ice stream. In other words, the profile reflects a larger vertical advection than expected from accumulation alone.

The Jakobshavn profile was taken from the side of a rapidly flowing ice stream. It illustrates an extreme case of the influence of horizontal advection. As ice flows rapidly toward the edge of the ice sheet, the surface steepens and the surface temperature increases rapidly. Heat dissipation in deforming ice warms the bed too (Section 9.7.1.1). The core of cold ice in between does not have time to warm, however.

Temperature gradients at the bed are about $0.022\,^{\circ}\mathrm{C\,m^{-1}}$ at Vostok and $0.053\,^{\circ}\mathrm{C\,m^{-1}}$ at Bindschadler Ice Stream. A geothermal flux of $50\,\mathrm{mW\,m^{-2}}$ produces a temperature gradient of $0.024\,^{\circ}\mathrm{C\,m^{-1}}$ in ice. However, measurements of basal temperature gradients do not give reliable estimates of geothermal flux without extensive analysis. Frictional heat must be accounted for. Even in the deepest boreholes, the history of climate change affects the basal temperature gradient. Analyzing the temperature profiles in detail requires time-dependent models. The variations of temperature in the upper parts of the GISP2 and Byrd profiles largely reflect past climate changes, though some cooling from horizontal advection is also apparent at Byrd.

9.7 General Equation of Heat Transfer

9.7.1 Derivation of Equation

This analysis follows Paterson and Clarke (1978). The base of the glacier is assumed to be horizontal. As before, the origin sits at the base, with x-axis horizontal and z-axis vertical, positive upward. Choose the y-axis so as to make the system right-handed. The coordinate system is fixed in space.

The equation of conservation of energy in a deforming medium can be written

$$\rho \frac{DE}{Dt} = \dot{S}_E - \frac{\partial q_x}{\partial x} - \frac{\partial q_y}{\partial y} - \frac{\partial q_z}{\partial z} \tag{9.25}$$

(Malvern 1969, pp. 226–231). Here E is internal energy per unit mass, $\dot{S}_E$ the source rate of heat per unit volume, $\vec{q}$ the heat flux vector due to conduction, ρ the density, and t time. D/Dt denotes differentiation following the motion, so that

$$\frac{DE}{Dt} = \frac{\partial E}{\partial t} + u\frac{\partial E}{\partial x} + v\frac{\partial E}{\partial y} + w\frac{\partial E}{\partial z} \tag{9.26}$$

for ice velocity components u, v, w.

In ice sheets, the only component of internal energy that changes significantly is thermal; thus $DE/Dt = c\,[DT/Dt]$, where T denotes temperature and c is specific heat capacity. Heat flux by conduction, in direction x, amounts to $q_x = -k_\mathrm{T}\partial T/\partial x$ for thermal conductivity k_T. Thus

$$-\frac{\partial q_x}{\partial x} = k_\mathrm{T}\frac{\partial^2 T}{\partial x^2} + \frac{\partial k_\mathrm{T}}{\partial x}\frac{\partial T}{\partial x}. \tag{9.27}$$

Similar relations give the y and z components. Thermal conductivity varies with position because it depends on density and temperature. Variation in the z-direction predominates; we neglect variation in other directions. Thus

$$\begin{gathered}\frac{\partial k_\mathrm{T}}{\partial x} = \frac{\partial k_\mathrm{T}}{\partial y} = 0 \\ \frac{dk_\mathrm{T}}{dz} = \frac{\partial k_\mathrm{T}}{\partial \rho}\frac{\partial \rho}{\partial z} + \frac{\partial k_\mathrm{T}}{\partial T}\frac{\partial T}{\partial z}.\end{gathered} \tag{9.28}$$

Equation 9.25 then becomes

$$\rho c\frac{\partial T}{\partial t} = k_\mathrm{T}\nabla^2 T - \rho c\left[u\frac{\partial T}{\partial x} + v\frac{\partial T}{\partial y}\right] + \left[\frac{dk_\mathrm{T}}{dz} - \rho c w\right]\frac{\partial T}{\partial z} + \dot{S}_E \tag{9.29}$$

with dk_T/dz given by Eq. 9.28. This is the general equation for heat transfer in ice sheets. Note that the dependence of k_T on T makes the equation nonlinear. The terms $\partial k_\mathrm{T}/\partial T$ and $\partial k_\mathrm{T}/\partial \rho$ can be evaluated from Eqs. 9.2 through 9.4. The temperature dependence matters most near the

base of an ice sheet, the location of steepest temperature gradients and smallest w. The term dk_T/dz reinforces the downward advection, reducing basal temperatures slightly below those calculated with a constant value of k_T. The density dependence of k_T is significant in the firn, but nowhere else.

9.7.1.1 Heat Sources

The term $\dot{S}_E$ in Eq. 9.29 consists of heat produced by (1) ice deformation, (2) firn compaction, and (3) freezing of water. The latter two occur primarily near the surface, although (3) sometimes occurs at depth.

Ice Deformation Consider an element with sides of length Δx, Δy, Δz. Applying a stress σ_{zz} causes the sides Δz to lengthen by an amount $\delta z = \epsilon_{zz}\Delta z$, given a strain ϵ_{zz}. The work done to accomplish the strain is $\left[\sigma_{zz}\Delta x\Delta y\right]\delta z$. All of this work converts to heat. Thus the rate of heat production, per unit volume per unit time, is $\dot{\epsilon}_{zz}\sigma_{zz}$, where $\dot{\epsilon}_{zz}$ is the strain rate in the z direction. The rate of heat production totals

$$\dot{S}_E^{(1)} = \dot{\epsilon}_{xx}\sigma_{xx} + \dot{\epsilon}_{yy}\sigma_{yy} + \dot{\epsilon}_{zz}\sigma_{zz} + 2\left[\dot{\epsilon}_{xy}\sigma_{xy} + \dot{\epsilon}_{xz}\sigma_{xz} + \dot{\epsilon}_{yz}\sigma_{yz}\right]. \tag{9.30}$$

The factor 2 arises because both of the symmetrical components of each shear stress do work (for example, σ_{xy} and σ_{yx}). In solid ice, but not firn, incompressibility means that the hydrostatic pressure does no work; the stresses can be replaced by their deviatoric counterparts. In the more compact form of indicial notation, an alternative expression is thus $\dot{S}_E^{(1)} = \dot{\epsilon}_{jk}\tau_{jk}$.

Deformational heat production concentrates where both deviatoric stresses and strain rates are highest – usually in basal layers but also in lateral shear margins. For example, measured temperature profiles part way through the rapidly shearing margins of Whillans Ice Stream show significant warming (Harrison et al. 1998).

Firn Compaction Changes in firn density at a fixed depth below the surface are usually small compared to the changes experienced by a given layer of firn during burial. In a steady-state ice sheet, a fixed depth corresponds to a point fixed in space. Mass conservation then requires that $\nabla\cdot\left[\rho\vec{u}\right] = 0$, given a velocity vector $\vec{u}$. Since density variations in the x- and y-directions are trivial, this reduces to

$$-w\frac{d\rho}{dz} = \rho\nabla\cdot\vec{u} = \rho\left[\dot{\epsilon}_{xx} + \dot{\epsilon}_{yy} + \dot{\epsilon}_{zz}\right]. \tag{9.31}$$

The hydrostatic component dominates stresses in firn, and so $\sigma_{xx} = \sigma_{yy} = \sigma_{zz} = -P$, with

$$P = g\int_z^{z_s} \rho\left(z'\right)dz'. \tag{9.32}$$

Therefore, by Eq. 9.30, compaction produces heat at a rate

$$\dot{S}_E^{(2)} = \frac{w P}{\rho} \frac{d\rho}{dz}. \tag{9.33}$$

Refreezing of Surface Water in Firn Refreezing liberates latent heat at a rate, per unit volume and time, of

$$\dot{S}_E^{(3)} = L w_s \rho_s m_f / z_m. \tag{9.34}$$

Here suffix s indicates surface values, m_f indicates the *melt fraction* – the fraction of the annual firn layer, by weight, formed by refreezing of water – and z_m is the maximum depth to which water penetrates. The refrozen water is assumed to be distributed uniformly over the layer. One small additional term is the heat released as the refrozen water cools to the temperature of the surrounding firn (Paterson and Clarke 1978; Eq. 9.16). The value of m_f, as a function of depth, can be measured in an ice core.

Heat of Sliding Friction Because this enters the glacier as a heat flux at the base, not by internal heat production, it is not included in the term $\dot{S}_E$. The flux equals the product of displacement and resistive force at the glacier bed, per unit time and area:

$$q_b = u_b \tau_\mathrm{b}, \tag{9.35}$$

with u_b and τ_b the magnitudes of basal slip and shear stress, respectively. If $\tau_\mathrm{b} = 100\,\mathrm{kPa}$, this flux matches a typical geothermal flux for u_b in the range 15 to $20\,\mathrm{m\,yr^{-1}}$. Slip rates of large glaciers commonly exceed this range.

Geothermal Heat Average fluxes on the continents range from $46\,\mathrm{mW\,m^{-2}}$ for rocks more than 1700 Myr old to $77\,\mathrm{mW\,m^{-2}}$ for rocks younger than 250 Myr (Sclater et al. 1980). Typical values depend on the tectonic setting. Extensional provinces, like the Basin and Range of western North America, have elevated geothermal heat fluxes (70 to $80\,\mathrm{mW\,m^{-2}}$). Parts of the West Antarctic Ice Sheet overlie a similar province. Indeed Engelhardt (2004a) estimated a geothermal flux of $69\,\mathrm{mW\,m^{-2}}$ from analysis of the Siple Dome borehole temperature profile. Similar analyses in central Greenland found a geothermal flux of $53\,\mathrm{mW\,m^{-2}}$ (Dahl-Jensen et al. 1998). Direct estimates of the geothermal flux beneath ice sheets have only been obtained in a few locations worldwide.

Very much higher geothermal heat fluxes occur locally, on or near volcanic centers. Analyses of melt rates indicate fluxes as high as $7\,\mathrm{W\,m^{-2}}$ on Mount Wrangell, Alaska, and as high as $50\,\mathrm{W\,m^{-2}}$ on Vatnajökull, Iceland (Clarke et al. 1989; Björnsson 1988). In north-central Greenland, the North-GRIP ice coring project discovered a previously unknown region of enhanced melt and heat flux beneath the ice sheet; the heat flux ranges from about 100 to $150\,\mathrm{mW\,m^{-2}}$ at the core site to more than $1\,\mathrm{W\,m^{-2}}$ nearby (NGRIP 2004; Fahnestock et al. 2001). The former value was obtained from analysis of the measured temperature profile; the latter, from melt rates inferred by down-warping of internal layers seen in radar soundings.

9.7.2 Boundary and Basal Conditions

At the surface, temperature is prescribed as a function of time. In contrast, neither the temperature nor the heat flux at the base of the glacier can be prescribed except in special cases. In the general case, the domain for temperature calculations must extend well into the substrate, to a depth that increases with the timescale considered. At the bottom of the domain, temperature or heat flux is held constant. To prescribe the latter, the temperature gradient is usually set equal to the heat flux divided by the thermal conductivity of the substrate material. This assumes a negligible transport of heat by any circulating fluids.

Three possibilities for conditions at the base of the ice are:

1. For a temperature below melting point, the gradient in the ice often approximates the value expected for a steady state:

$$\left[\frac{\partial T}{\partial z}\right]_B \approx -\frac{G}{k_{\mathrm{T}}} \tag{9.36}$$

for a geothermal flux G. In general, however, the basal gradient changes as temperature transients pass through the bed or the glacier advances onto new terrain. Note that, with z pointing upward, the steady gradient is a negative quantity.

2. If the ice reaches melting point (T_m) only at the glacier base:

$$T_B = T_m \quad \text{and} \quad \left[\frac{\partial T}{\partial z}\right]_B < \frac{\partial T_m}{\partial z}, \tag{9.37}$$

where, given that $\mathcal{B} = 7.42 \times 10^{-8}\,^{\circ}\mathrm{C\ Pa^{-1}}$, the maximum (positive) gradient is $\partial T_m/\partial z = \mathcal{B}\rho g \approx 7 \times 10^{-4}\,^{\circ}\mathrm{C\ m^{-1}}$. For comparison, note that some of the measurements discussed in Section 9.6 obtain values for $[\partial T/\partial z]_B$ as low as $-0.057\,^{\circ}\mathrm{C\,m^{-1}}$. The rate of basal melt or freeze-on, corresponding to the basal specific mass balance $\dot{b}_b$ (dimensions of length per unit time), can be calculated from (see Chapter 4):

$$-\rho_i L\dot{b}_b = G + \tau_{\mathrm{b}} u_{\mathrm{b}} + k_{\mathrm{T}}\left[\frac{\partial T}{\partial z}\right]_B. \tag{9.38}$$

In other words, a net heat flow to the bed – a positive value for the sum on the right-hand side – causes melt, a negative specific balance.

3. Within a basal layer of temperate ice,

$$T = T_m \quad \text{and} \quad \frac{\partial T}{\partial z} = \frac{\partial T_m}{\partial z}. \tag{9.39}$$

Its upper boundary corresponds to the lowest level at which $\partial T/\partial z < \partial T_m/\partial z$. The reversed temperature gradient in the temperate layer prevents the inflow of frictional and geothermal heat; all such heat melts ice at the base, according to Eq. 9.39. The existence of the

layer, and all melting within it, results from the heat of ice deformation (Eq. 4.13). All the meltwater is assumed to drain away; otherwise the temperate ice has to be treated as a mixture of ice and water, which increases the complexity of the analysis (Hutter 1982).

9.8 Temperatures Along a Flow Line

Dahl-Jensen (1989) calculated how the steady temperature distribution varies along a flow line in an ice sheet. Her method simultaneously solved the equations for heat flow and ice flow. Only the temperature results are presented here; the corresponding stress and velocity distributions are discussed in Section 8.7.

The assumptions are steady-state, two-dimensional flow, no firn, constant thermal conductivity, internal heating only from shear. Equation 9.29 then reduces to

$$u\frac{\partial T}{\partial x} + w\frac{\partial T}{\partial z} = \alpha_{\mathrm{T}}\left[\frac{\partial^2 T}{\partial x^2} + \frac{\partial^2 T}{\partial z^2}\right] + \frac{2}{\rho c}\dot{\epsilon}_{xz}\tau_{xz}. \tag{9.40}$$

The bed is assumed to be horizontal. At the surface, as elevation drops along the flow line, the specific balance decreases and the temperature increases at prescribed rates. Values of ice thickness, surface temperature, geothermal flux, accumulation, and ablation resemble those for southern Greenland (Figure 8.23). The velocity components are determined, as functions of position, from the solution of the equations for ice flow. All equations are solved numerically.

Figure 9.8 shows computed temperatures along the flow line. The main features are:

1. Basal temperature increases with distance from the ice divide because both surface temperature and heat of deformation increase.

2. Basal melting starts at $X = 0.625$. (Here X denotes the distance along the flow line expressed as a fraction of total length.) The basal temperature gradient, hitherto increasing with X, starts to decrease because some heat goes to melting.

3. A temperate basal layer starts to form at $X = 0.75$, still in the accumulation zone. It first thickens with increasing X but then thins to zero as deformational heating declines near the terminus. (Along a fast-flowing outlet glacier, in contrast, heating would presumably remain important all the way to the front.)

4. Horizontal advection produces a minimum in the vertical profile of temperature. This cold spot strengthens and persists along the flow line, as far as the outer ablation zone.

5. The temperature profile near the terminus resembles that predicted for an ablation zone by Robin's simple analysis (the curve for $\gamma = -3$ in Figure 9.5).

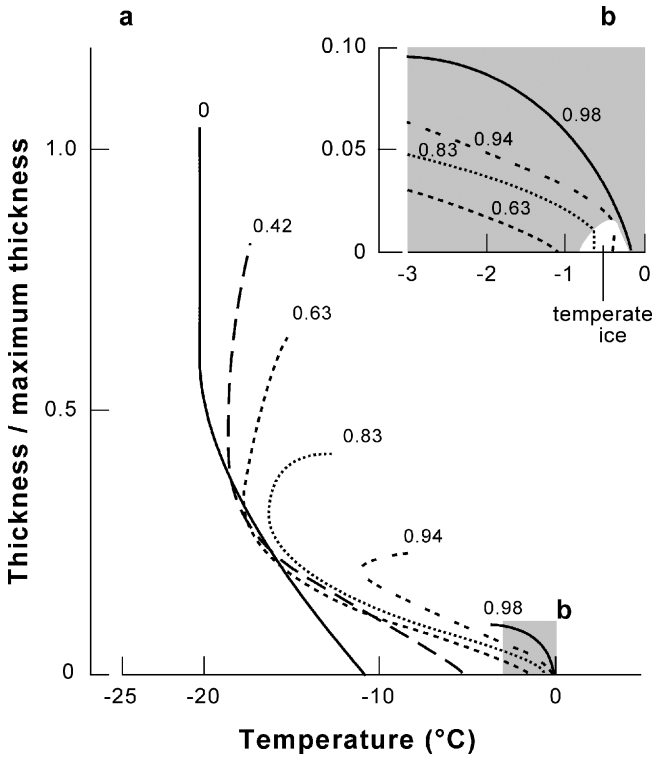

Figure 9.8: (a) Theoretical temperature profiles along an ice sheet flow line. The number on each curve is the distance as a fraction of the flow-line length. The equilibrium line is at 0.91. (b) Closer view of profiles near the margin. A temperate layer develops at the bottoms of profiles 0.83 through 0.98. Adapted from Dahl-Jensen (1989) and used with permission of the American Geophysical Union, *Journal of Geophysical Research*.

9.8.1 Observations

A series of temperature profiles along a flow line has never been measured in an ice sheet. However, Figure 9.9 shows temperature profiles measured along the centerline of White Glacier, a polar glacier on Axel Heiberg Island, Canada. Conditions in this valley glacier, which is 15 km long, differ from those assumed in the theoretical analysis in several ways:

1. The glacier is not in a steady state.
2. The bed has an average slope of 6°.
3. The ice thickness varies with distance in an irregular way.

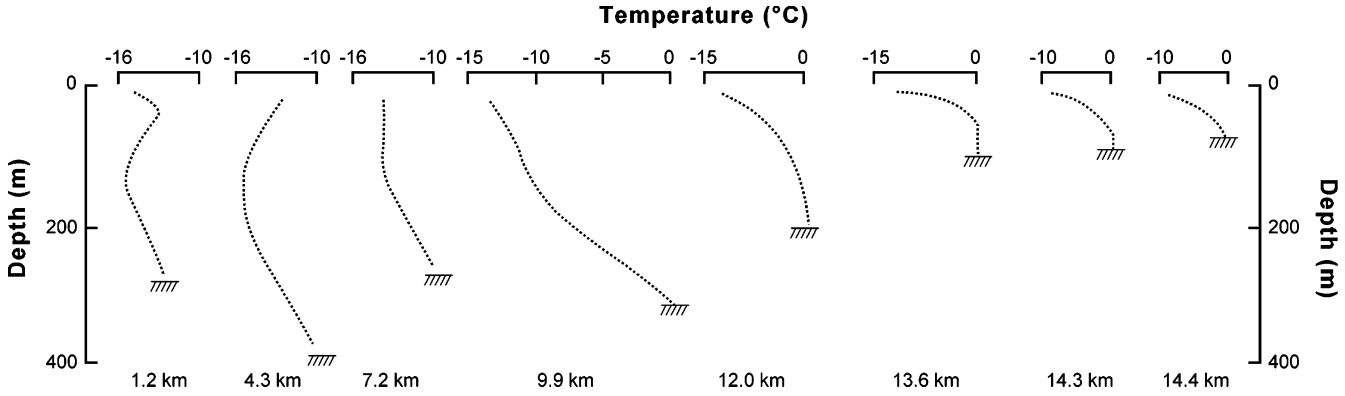

Figure 9.9: Temperature profiles in White Glacier, at various distances along the flow line. Depth to bed is indicated in each case. Note change in temperature scale between 9.9 and 12 km. Data from Blatter (1985).

4. The 10 m ice temperature does not increase steadily with X.
5. The ablation zone is proportionately much larger.

Nevertheless the data show most of the predicted features:

1. An increase in basal temperature with distance down-glacier.
2. A temperate basal layer, in this case restricted to the ablation zone, that does not extend to the terminus.
3. Profiles of the predicted shape near the terminus.
4. A temperature minimum extending into the ablation zone. However, the minimum appears in the first profile, only 1.2 km from the head of the glacier. Thus the cool spot probably represents, in part, a remnant of low temperatures during the Little Ice Age and not just the effects of horizontal advection (Blatter 1987).

Temperate basal layers have also been observed in Laika Glacier and Barnes Ice Cap, Arctic Canada (Blatter and Kappenberger 1988; Classen 1977), and near the ice edge in west Greenland (Stauffer and Oeschger 1979), including the lateral margins of the Jakobshavn Ice Stream (Lüthi et al. 2002).

9.9 Time-varying Temperatures

Steady-state models explain many of the prominent features of temperature profiles, but no real ice sheet is ever in a steady state. Changes of temperature at depth originate with changes of surface temperature, water infiltration, vertical ice flow, horizontal ice flow, and ice thickness. Other factors, such as variations of geothermal flux, are less important in general but locally important.

As Table 9.2 shows, the temperature variations during the 100 kyr ice-age cycle could penetrate through the deepest ice sheets by conduction alone. Advection increases the penetration. The basal temperature gradient therefore changes with time, and calculations must include heat transfer in a bedrock layer of comparable thickness to the ice. In addition, computations have to span a period long enough for the system to "forget" the assumed initial temperature distribution. For ice sheets, this takes several glacial cycles. Most analyses of time-varying temperature distributions require numerical methods.

The response at depth to a time-varying surface temperature can be illustrated with the simple case of an abrupt climate warming. Consider a step increase of surface temperature; that is, the surface temperature maintains a constant, cold value for a long time and then abruptly increases to a warmer value that persists. A wave of warming then propagates downward into the ice sheet by conduction and advection. Figure 9.10 illustrates a calculation of this scenario, a solution to Eq. 9.29 for an ice divide (no horizontal advection) with a constant thickness (of 3 km) and

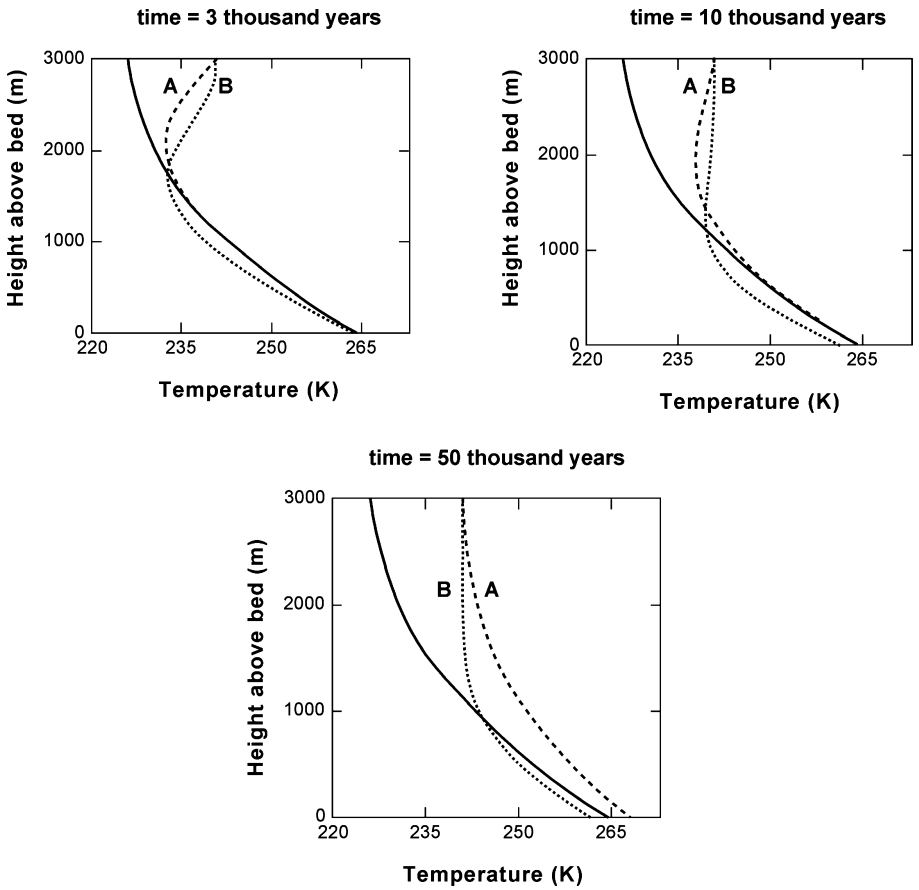

Figure 9.10: Propagation of a temperature wave following a 15 °C step increase of surface temperature at time zero. The initial curve (solid line in all panels) is a steady-state profile for an accumulation rate of 0.07 m yr^{-1}. In all three panels, Case A assumes no change in the vertical ice velocity from the initial state. In Case B, the vertical velocity increases to 0.3 m yr^{-1} at time zero.

density, overlying a 3-km-thick bedrock slab. The temperature profile begins in a steady state, adjusted to parameters appropriate for central Greenland in an ice-age climate. The downward vertical velocity is assumed to equal 0.07 m yr^{-1} at the surface, decreasing linearly to zero at the bed. The curves labelled "A" show the response if the vertical velocity remains constant. If, however, the same temperature change is accompanied by an increase of vertical velocity, to 0.3 m yr^{-1} (surface value), the warming propagates more rapidly (curves "B" in the figure). But the increased advection also causes cooling of the deeper ice, despite the warmer surface. This second scenario is the more realistic one for polar ice sheets, because snowfall increases at transitions to warmer climates, leading to increased vertical velocities. Ice thickness increases for the same reason, a process that, acting alone, leads to warming of deep ice. This opposes

the advective cooling (Ritz 1987). But climate warming also results in retreat of the ice sheet's margins, a process that ultimately thins the entire ice sheet (Section 11.4.2.2).

Inspection of Figure 9.10 shows that even ten millennia after the warming event a cold spot persists at depth – a legacy of the earlier, colder climate. Ice sheet temperature profiles taken now, roughly ten millennia after the end of the last ice age, should contain such a signature. Indeed, such cold spots are observed, most clearly in borehole temperature measurements from the Greenland Ice Sheet (Dahl-Jensen and Johnsen 1986; Cuffey et al. 1995).

Climate change entails irregular variations of temperature and accumulation rate over time. Ice cores provide an opportunity to reconstruct the histories of both (see Chapter 15). Such information allows comparisons of measured borehole temperature profiles with predictions from the heat-transfer equation (Johnsen 1977b; Paterson and Clarke 1978; Cuffey and Clow 1997; Lhomme et al. 2005). Ice thickness changes need to be modelled as part of the analysis.

Paterson and Clarke (1978) studied temperatures in a 299-m borehole through the Devon Island ice cap, using the oxygen-isotope record back to 11 kyr B.P. as a measure of surface temperature. They showed that no steady-state model could fit their data well, whereas the model driven by the isotope record matched the data to within 0.04 °C. Their analysis did not include ice thickness changes, but more recent ones have. Cuffey et al. (1995) analyzed the temperature profile from a 3.05-km-deep borehole in central Greenland, using a 100 kyr oxygen-isotope record (δ) to constrain surface temperature and other ice core information to constrain accumulation rate ($\dot{b}_i$). Ice thickness variations were estimated from $dH/dt = \dot{b}_i - w_s$, using a simple ice flow model to calculate w_s. Their calculated temperatures matched the borehole temperature data to within 0.1 °C, provided that the value for isotopic sensitivity (Chapter 15), $\alpha_\star = d\delta/dT$, was adjusted. The value needed for a good match, $\alpha_\star = 0.33$ per mil °C^{-1}, was significantly smaller than the one normally assumed. Using the "normal" value of $\alpha_\star = 0.67$ gave a difference between modelled and measured temperatures of as much as 1 °C. The results were not sensitive to the ice-flow model used to calculate w_s because the depth-age relation for the ice core provided an additional constraint on the vertical displacement of layers.

Lhomme et al. (2005) performed a similar analysis but using a three-dimensional model for the entire Greenland Ice Sheet to constrain flow and thickness changes. The lower resolution of this model reduced the match to the measured temperature profile, but the fit was still good. Moreover, the method permitted a simultaneous comparison between predictions and measurements at multiple sites; specifically, the depth-age relation was calculated for the whole ice sheet and compared to the measured relations at three ice core sites. Good matches were achieved. Salamatin et al. (1998, 2008) analyzed temperatures in the Vostok borehole, East Antarctica, using an approach similar to Cuffey et al. (1995), and achieved a close match to the measured temperatures. The good performance of all these models gives some confidence that the heat-transfer process is well understood and confirms the accuracy of the general pattern of climate changes inferred from ice cores.

Temperature-wave propagation, such as that illustrated by Figure 9.10, occurs throughout an ice sheet after a climate change. In addition, temperatures adjust any time ice flow changes

(which alters heat generation and horizontal advection) and whenever the ice sheet thickens or thins. The evolving three-dimensional temperature field is simulated routinely as a component of whole-ice-sheet model calculations; for example, Huybrechts (1996) discussed results for temperatures at the bed of the Greenland Ice Sheet throughout a glacial climate cycle. In such models, temperatures must be calculated because they influence both the ice viscosity and the spatial pattern of basal slip. The simulated temperatures are not well constrained by data, however. More borehole measurements of temperature are keenly needed, not just at ice divides but also on ice sheet flanks.

The only region of an ice sheet flank with temperature measurements in multiple boreholes to the bed is the Siple Coast sector of West Antarctica, a region of fast-flowing ice streams separated by slow-flowing ice ridges (Section 8.9.2.4). The temperatures reveal a complicated thermal legacy of major recent changes of the ice flow. The temperature profile through one of the ridges, Siple Dome, is close to a steady state, with a minor influence from warming at the end of the last ice age (Engelhardt 2004a). Profiles through two ice streams (Kamb and Bindschadler) show the signature of fast glacier flow: strong cooling from horizontal advection at mid-depths and frictional warming near the bed (Figure 9.6; Joughin et al. 2004c; Engelhardt 2004b). But observations show the same type of profile in a large region of stagnant ice (called "the Unicorn"). Other evidence indicates that this region stagnated only two centuries ago (Clarke et al. 2000); the temperature profile is clearly a relict from an extended period of fast flow prior to stagnation. So too with the profile from Kamb Ice Stream, a feature that nearly stagnated a few centuries ago (Retzlaff and Bentley 1993). In contrast, the temperature profile in part of one actively flowing ice stream (B2) adjacent to the Unicorn resembles the profile in the ridge Siple Dome; this indicates that only recently was the ice of B2 entrained in the fast-flowing stream. The Siple Coast region thus contains a startling array of examples of major thermal disequilibrium.

The interaction of ice flow and temperature and the long legacy effects possible in ice due to slow heat conduction suggest that a lot of new information can be gained from analyzing borehole temperature measurements specifically acquired for ice dynamic analyses. Nereson and Waddington (2002) theorized one example. If an ice divide moves, the warm spot beneath it (Section 9.5.1.1) should dissipate only slowly. Migration of an ice divide should therefore leave a thermal trace that might be measured.

9.10 Temperatures in Ice Shelves

How do temperatures vary in a floating ice shelf? At the base of a shelf, the temperature is fixed by the freezing point of seawater, and the heat flux depends on the temperature, salinity, and circulation of the seawater underneath. The flux determines whether ice melts from the shelf or seawater freezes to it. (We have discussed the basal mass balance of ice shelves in Section 4.5.) For a steady state, the vertical velocity component at the base must compensate for the melting or accretion. Ice shelves are fed by glaciers emanating from inland ice sheets; for some distance into

the shelf the temperatures reflect the values inherited from the inland ice. Thinning of the shelf as the ice flows out to sea also affects the temperature distribution. Shumskiy and Krass (1976) made a detailed general analysis, treating heat and ice flow simultaneously. They calculated steady-state temperature profiles. Humbert et al. (2004) used a three-dimensional numerical calculation to simulate the coupled heat and ice flow in the Ross Ice Shelf, the world's largest.

Figure 9.11 shows measured temperatures in ice shelves. Data sources are Maudheim (Schytt 1954), Little America (Bender and Gow 1961), Amery (Weeks and Mellor 1978), J9 (Clough and Hansen 1979), and Filchner (Dyurgerov et al. 1988). The measurements have been extrapolated to $-2\,^{\circ}\mathrm{C}$, an estimate for freezing temperature of seawater at the base. The different shape of the Amery curve results from basal freezing (Morgan 1972) in contrast to basal melting at Maudheim, Filchner, and Little America. Because the lowest 6 m of the core from J9 was salty (Jacobs et al. 1979), seawater must be freezing to the shelf upstream, but the rate of accretion is not known. Where melting prevails, the basal temperature gradients are large; at Little America, for example, the gradient amounts to about 15 times a normal geothermal gradient. Melting erodes the basal layers of the shelf, bringing warm seawater in contact with cold ice in the core of the shelf. The resulting steep gradient draws heat from the underlying seawater. For melt to continue, the heat must be continually supplied by circulation of the water beneath the shelf.

Detailed interpretation of the individual curves is difficult because the temperature distribution depends on conditions upstream as well as at the borehole. The report by MacAyeal and Thomas (1979) exemplifies an analysis that tries to account for all the relevant factors. They

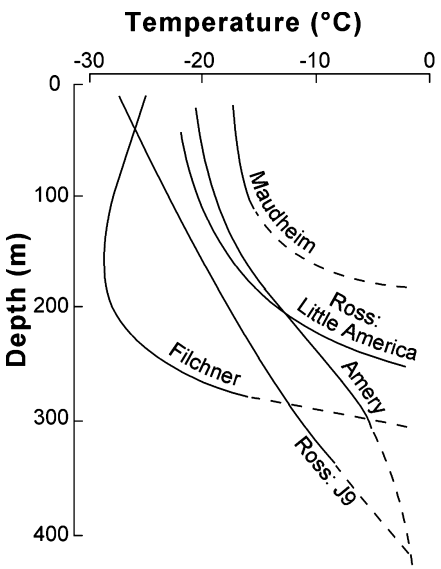

Figure 9.11: Temperature profiles in ice shelves. Broken lines indicate extrapolations. Data sources are given in the text.

obtained a good fit to the measurements for J9 by using a nonsteady-state numerical model that accounts for conditions along the flow line from the ice-shelf grounding line to the borehole.

Temperature variations along-flow and across-flow on ice shelves are not known well from the limited number of borehole studies. Because temperature affects ice viscosity, however, internal temperature distributions leave a mark on the pattern of ice flow throughout a shelf. A surface velocity map of a shelf therefore contains information about temperature. Larour et al. (2005) analyzed extensive flow data for the Ronne Ice Shelf to determine patterns of ice viscosity variation. They showed that the side margins are softer and hence warmer than elsewhere, an expected consequence of concentrated frictional heating where the ice shears rapidly. They also inferred colder and stiffer ice where major glaciers leave the continent and enter the shelf.